Available online at www.sciencedirect.com
SCIENCE DIRECT®
Journal of Colloid and Interface Science 269 (2004) 171–177
JOURNAL OF Colloid and Interface Science
www.elsevier.com/locate/jcis

Advancing contact lines on chemically patterned surfaces

T. Cubaud * and M. Fermigier

Laboratoire PMMH, CNRS UMR 7636, ESPCI, 10, rue Vauquelin, 75231 Paris cedex 05, France

Received 24 March 2003; accepted 4 August 2003

Abstract

We report an experimental investigation on advancing contact lines of large drops spreading on chemically patterned surfaces. The model substrates were prepared using microphotolithography allowing precise control of the position and the size of the wettability patterns. Experiments were performed exploring different surface geometries: from ordered to disordered fields of defects and from low to high surface densities. The shape of the contact line between two isolated defects was investigated as a function of the distance. Portions of the contact line on the defects and on the matrix were studied during spreading experiments and were related to the apparent contact angles measured from the final thickness of the drops. A modified Cassie equation based on the line fraction of defects is proposed.

Keywords: Partial wetting; Contact line; Contact angle; Hysteresis; Heterogeneous; Defects; Cassie; Patterned

1. Introduction

Wetting phenomena often take place on nonideal surfaces and have a wide range of applications from oil recovery, offset printing [1], and biology [2] to microfluidics [3].

The contact angle is the angle made by a liquid (l) on a solid (s) in contact with a gas (g). The Young–Laplace equation predicts a unique value for the equilibrium contact angle θ_e as a function of the three interfacial energies γ_{sl} (γ), γ_{sg}, and γ_{lg}:

$$\cos\theta_e = \frac{\gamma_{\mathrm{sg}} - \gamma_{\mathrm{sl}}}{\gamma}. \tag{1}$$

Experimentally, the static contact angle θ_s and the equilibrium contact angle θ_e are different. The static contact angle θ_s ranges from the receding contact angle θ_r to the advancing contact angle θ_a depending on the previous history of the system. On a heterogeneous surface, the contact angle varies along the contact line $\mathcal{L}$ and depends on the position of the line on the substrate. The existence of hysteresis means usually that a system is trapped in a metastable state. As a heterogeneous surface presents multiple local minima of the total free energy of the system, the contact line may be trapped on positions separated by strong energy barriers. The equilibrium contact angle θ_e associated with the absolute minimum of energy can be obtained adding external energy to the system [4,5]. The deformation of the contact line due to a single wettability defect and multiple defects was experimentally investigated in a capillary rise situation [6–8], in an imperfect Hele-shaw cell [9], for drops squeezed between solid surfaces [10], and for liquid-He films [11].

In this paper we examine the deformation of the contact line of large drops spreading on heterogeneous surfaces. Large drops resting on a solid surface are flattened by gravity. The flat surface is limited by a meniscus the size of which is determined by the capillary length $\lambda_c = \sqrt{\gamma/\rho g}$ where ρ is the liquid density and g is the gravity acceleration (see Fig. 1). We first describe the contact line structure on a single defect. For the case of many defects, the radius of curvature of the contact line between two defects is measured and related to the distance between defects. As a function of the defect density on the substrate, individual pinning and collective pinning are observed. For a given density of defects, experiments show a single value of the mean advancing contact angle that does not depend on the nature of disorder. The mean or apparent contact angle θ_m averaging the different contact angles along the contact line $\mathcal{L}$ can be defined on a heterogeneous surface extrapolating a definition for a uniform substrate; θ_m is then a function of the mean thickness h_m of the drop [5]:

$$\theta_m = 2\arcsin\frac{h_m}{2\lambda_c}. \tag{2}$$

* Corresponding author.
E-mail address: cubaud@seas.ucla.edu (T. Cubaud).

0021-9797/$ – see front matter
doi:10.1016/j.jcis.2003.08.008

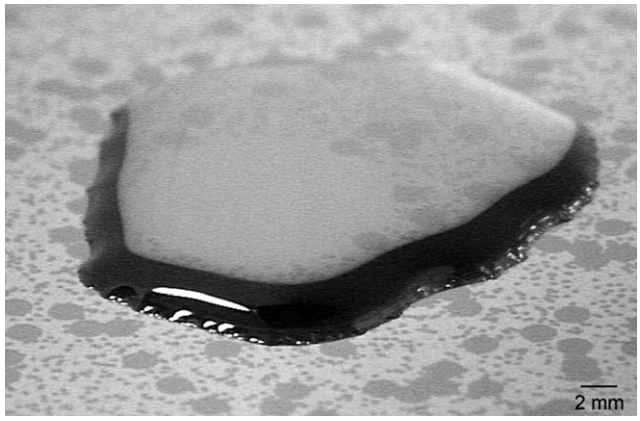

Fig. 1. Large sessile drop on model heterogeneous substrate.

Using this equation, the apparent contact angle θ_m is determined from h_m at the end of each experiment. Taking into account the local and the general surface geometry of the defect field, the apparent contact angle θ_m is shown to be predictable using a modified Cassie equation with the line fraction of defects.

2. Experimental apparatus

The wettability defects are made with a photosensitive resin using a microphotolithography technique described previously [9]. The defect pattern is generated on a computer and printed with a very high resolution laser printer on a transparent paper used as a mask. A thin layer of photoresist (0.5 μm) is spin coated on a 10-cm bare polished silicon wafer. The wafer is then exposed to UV light through the mask. The parts of the resin layer exposed to UV light are removed by immersion in a developer bath. The masks used to expose the resin and produce circular defects were generated using a square lattice of mesh L. Each cell of the lattice contains a defect. Its position within the cell involves a noise parameter N_0 so that the position (x, y) of a defect is

$$(x, y) = \begin{cases} x = L(i + N_0 r_x) \\ y = L(j + N_0 r_y), \end{cases}$$

where i and j are integers defining the cell number in the lattice and r_x and r_y are random numbers uniformly distributed between 0 and 1. By changing the value of the noise parameter we can go from a periodic distribution of defects ($N_0 = 0$) to a random distribution of defects ($N_0 > 1$) (defect fields with different noise parameters are displayed in Fig. 7).

The defect density on the substrate is defined via the surface fraction of defects σ, which is the ratio of the surface occupied by a circular defect of diameter d and the surface of the mesh of the lattice:

$$\sigma = \frac{\pi d^2}{4L^2}. \tag{3}$$

The defect density can also be defined with the mean line fraction of defects χ_m corresponding to the ratio of the diameter of a circular defect of diameter d in the mesh and the average length of a square mesh L_m,

$$L_m = \frac{4L}{\pi} \int_0^{\pi/4} \frac{1}{\cos\alpha}\, d\alpha \sim 1.12L, \tag{4}$$

and then,

$$\chi_m = \frac{d}{L_m}. \tag{5}$$

The line fraction of defects χ seen by the contact line depends on its position on the heterogeneous surface. In this paper we show experimentally that χ fluctuates around χ_m.

The liquid used is a mixture composed 60% glycerol and 40% water in volume. The capillary length for such a mixture is $\lambda_c = 2.44$ mm. Homogeneous substrates were used to measure the contact angles $\theta_{\text{matrix}} = 23^\circ$ on silicon and $\theta_{\text{defect}} = 61^\circ$ on resin. The wettability contrast $\Delta S = \gamma(\cos\theta_{\text{defect}} - \cos\theta_{\text{matrix}}) = 29.6$ mN/m is comparable in magnitude to the surface tension γ, allowing the influence of the defects to be clearly observed.

Figure 2 shows the experimental apparatus. The liquid is supplied into the drop using a syringe pusher at different flow rates ($Q = 9 \times 10^{-2}$, 23×10^{-2}, and 44×10^{-2} mm^3/s as a function of the size of the drop in order to maintain an average contact line velocity ranging from 1 to 10 μm/s, corresponding to a very small capillary number $Ca \sim 10^{-6}$). The substrate horizontality was set using a laser autocollimation technique and the drop evolution was monitored from above with a high-resolution camera (Kodak Megaplus 4.2i/10, 2032×2044 pixel^2, with 1024 gray levels). Using edge detection algorithms, the position of the contact line and the defects were determined at equally spaced times during the spreading. The combination of a large spatial resolution and a large range of gray levels allows a precise determination of the contact line position in relation to the position of each surface defect.

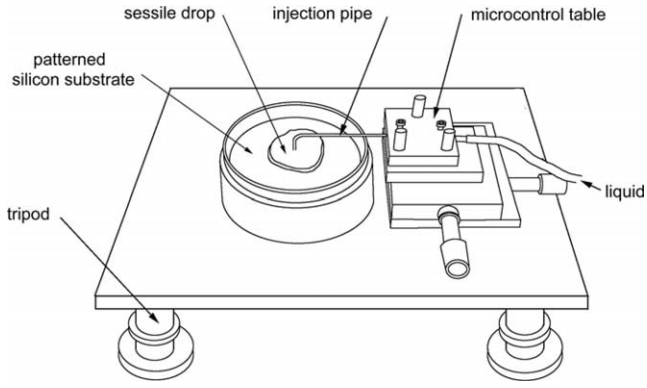

Fig. 2. Experimental setup.

3. Contact line structure

3.1. Single defect

The size of the defects $d = 0.1$ or 0.4 mm is larger in width than that of $\delta \sim$ a few nanometers of the three-phase contact area [12] ($d \gg \delta$). In this situation, the contact line $\mathcal{L}$ is a set of three-phase lines $\mathcal{L}_3$ (corresponding to a contact area lying on a homogeneous solid) and four-phase lines $\mathcal{L}_4$ (corresponding to a contact area lying at the border of two homogeneous solids). This can be analytically described by

$$\mathcal{L} = g(t)\mathcal{L}_3 + \big(1 - g(t)\big)\mathcal{L}_4, \tag{6}$$

where $g(t)$ is a function of time and surface geometry.

For a quasi-static motion, with a very small capillary number $Ca \ll 1$, the contact angle θ_3 of a three-phase line $\mathcal{L}_3$ can be considered unique. By definition, a four-phase line $\mathcal{L}_4$ is static but the associated contact angle θ_4 ranges between the contact angles on each solid, θ_{defect} and θ_{matrix}. Figure 3 illustrates this contact line property during the different stages of the pinning process on an isolated defect.

A defect on the path of the contact line deforms the line. If the defect and/or the wettability contrast is small enough (weak defect), the line recovers its unperturbed position after passing the defect. On the other hand, if the defect and/or the wettability contrast is too large (strong defect), the defect traps the line and stays uncovered by the liquid layer. The relevant parameter to describe the influence of a wettability defect is the dimensionless defect strength $f = \Delta S d/\gamma h_m$ corresponding to the ratio of the pinning force of the defect and the elastic restoring force of the meniscus. Previous experiments [13] have shown that in the case of weak defect ($f < 0.40$), the amplitude of deformation of the contact line on the transverse and on the direction of motion are proportional to the defect size.

3.2. Multiple defects

Figure 4a shows an oblique view of the edge of a large drop. Defects deform the liquid/gas interface on a distance

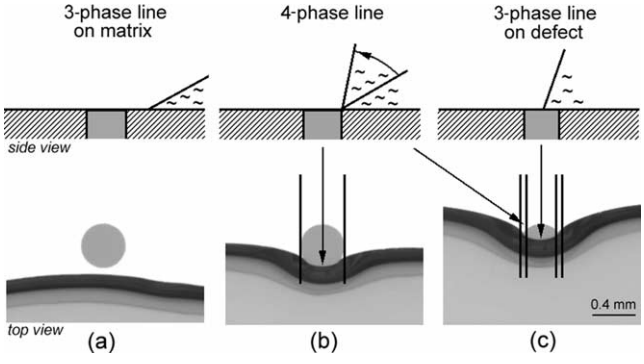

Fig. 3. Nature of the contact line during the pinning on an isolated defect: (a) three-phase line, (b) four-phase line around the defect, and (c) three-phase line on the defect, four-phase line on the edge of the defect.

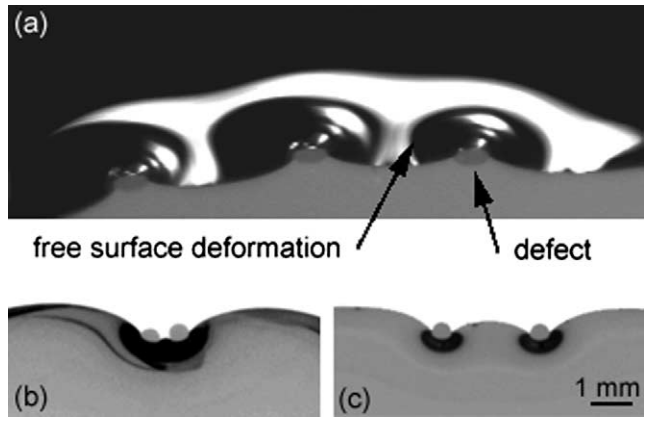

Fig. 4. Coupling between defects, $d = 0.4$ mm. (a) Oblique view of the edge of a large drop: 3D deformation. (b) Top view of the drop edge. Collective pinning, $L = 1.5d$. (c) Individual pinning, $L = 5d$. (The darker areas indicate a strong slope of the free surface.)

larger than their size. As a function of the distance L between the centers of the defects, the free surface deformations around two neighboring defects may merge as seen in Fig. 4b. To investigate the shape of the contact line between two defects, spreading experiments on a matrix with two defects of size $d = 0.4$ mm were performed varying L from $1.5d$ to $7d$ (see Fig. 5). The shape of the three-phase line $\mathcal{L}_3$ between two defects is fitted by an arc of circle just before the liquid starts spreading on the defects. Figure 5 shows the dependence of the radius of curvature R of the triple line $\mathcal{L}_3$ with respect to the distance L_r between the edges of the defects. The linear relation between R and L suggests that an effective capillary force of order $(\gamma/R)h_m L$ balances the defect force of order $d\Delta S$ before the spreading on defects. The ratio of the distance between defects L over the contact line

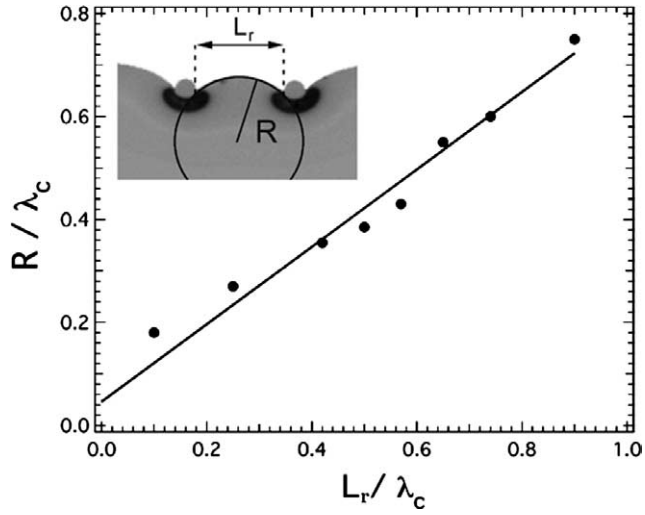

Fig. 5. Radius of curvature of the three-phase line as a function of the distance L_r between the centers of the defects, $d = 0.4$ mm. Lengths are normalized to the capillary length.

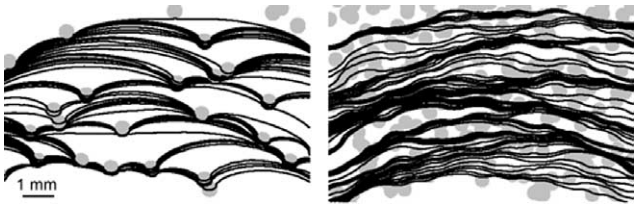

Fig. 6. Contact line time series on disordered defect distribution, $d = 0.4$ mm, $N_0 = 4$. Left: Individual pinning, $L_m = 3.5d$. Right: Collective pinning, $L_m = 1.25d$.

curvature R is constant in this experiment:

$$\frac{L}{R} \sim \frac{d\Delta S}{\gamma h_m}. \tag{7}$$

The influence of the defect size d and the wettability contrast ΔS on the contact line curvature between two defects will be investigated in further work.

For a field of defects, spreading experiments on surfaces with different surface fractions $0 < \sigma < 1$ have shown two main regimes for the contact line morphology as a function of L_m [14]. For a diluted distribution ($L > 2d$), defects act individually and the contact line can be assimilated in a first approximation to a set of arcs of circle pinned to the defects (see Fig. 6, left). For a dense distribution ($L < 2d$), close defects form clusters that pin the contact line for a longer period of time (see Fig. 6, right). This is the collective pinning regime. These regimes are characteristic of a moving elastic medium in a pinning potential [15]. It is important to note that the drop thickness, therefore the meniscus elasticity, depends on the contact angle distribution along the contact line related to the solid surface density of defects.

3.3. Transition to disorder

To characterize a heterogeneous surface density by a mean contact angle, constant density surfaces with different defect distributions were investigated.

Rectangular wettability channels (28×40 mm) were formed on the substrate with "walls" made with less-wetting lines. The liquid was injected at a closed end of the channel, and then the wetting front moved essentially along the two parallel lines 28 mm apart. For a constant surface fraction of defects $\sigma = 0.25$, square and hexagonal lattices were increasingly disordered, changing the noise parameter N_0 from 0 to 1. Figure 7 shows the time series of the contact line on a square lattice with a noise parameter (Fig. 7a) $N_0 = 0$ and (Fig. 7b) $N_0 = 1$. For a perfectly ordered lattice, (Fig. 7a) the contact line $\mathcal{L}$ is faceted by the first-neighbor axis of defects and (Fig. 7b) for a disordered distribution, the contact line $\mathcal{L}$ moves part by part as a function of the local clusters formed by close defects. The morphological transition between faceted and nonfaceted contact lines was described in a previous paper [13]. Using image processing, the time evolution of the wetted surfaces was measured (Fig. 8). For a constant flow rate ($Q = 9 \times 10^{-2}$ mm^3/s), the wetted surface shows a linear dependence in time. As

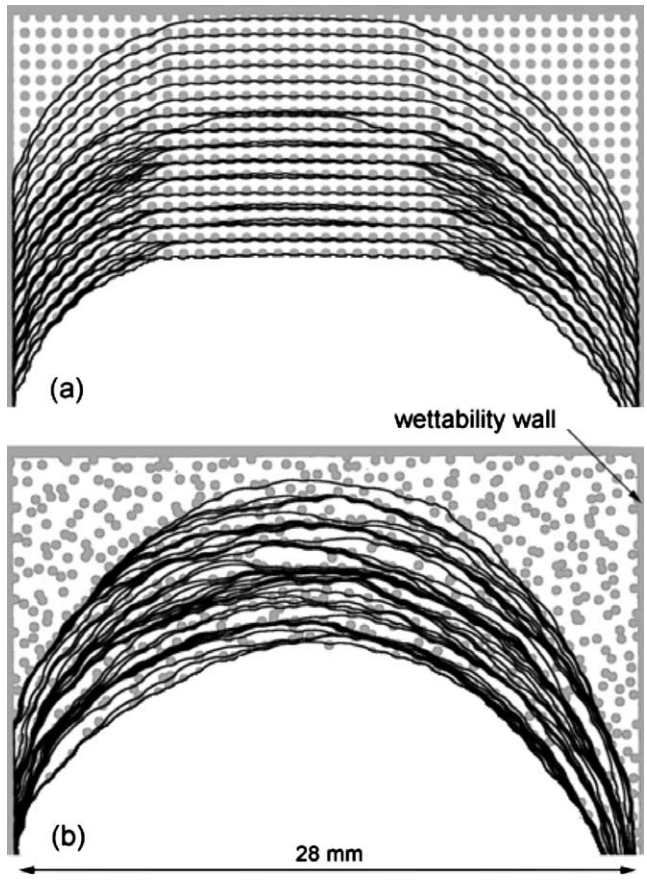

Fig. 7. Time series of the contact line on patterned wettability channels, $d = 0.4$ mm, $\sigma = 0.25$. (a) $N_0 = 0$, (b) $N_0 = 1$.

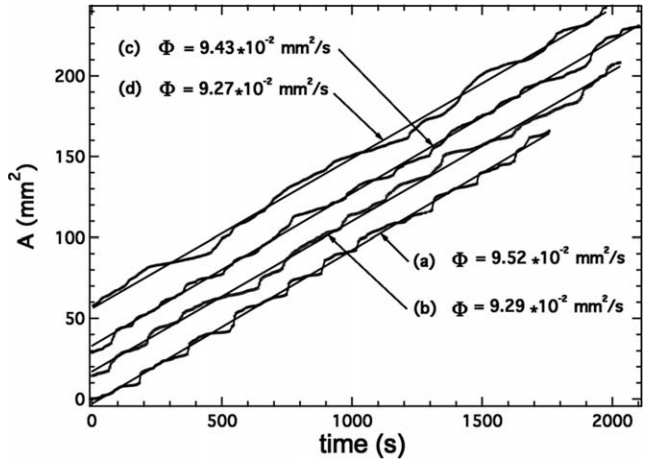

Fig. 8. Wetted surface vs time, $d = 0.4$ mm, $\sigma = 0.25$. (a) $N_0 = 0$, (b) $N_0 = 0.25$, (c) $N_0 = 0.5$, and $N_0 = 1$. (Curves are vertically shifted for a better view.)

the mean rate of growth of the wetted surface $\Phi = d\langle A\rangle/dt$ is the same in the four experiments, the mean thickness h_m of these drops is identical whatever the spatial distribution of defects is. If we relate the thickness of the advancing liquid puddle and the contact angle (Eq. (2)), as for a static sessile drop, we can define a unique apparent advancing con-

tact angle on such surfaces. These experiments show that although the contact angle depends on the position of the contact line $\mathcal{L}$, a unique apparent advancing contact angle can be associated with a given defect density independent of the line or the position of defects.

4. Contact angles

4.1. Defect density

Taking advantage of the high-resolution camera with 1024 gray levels, the line fraction of defects χ was determined as explained below:

Before each experiment, a snapshot $pix\,0$ of the solid surface was taken. A threshold was applied on the picture $pix\,0$ so that the defects appeared with a gray level n_d and the matrix appeared with a gray level n_s. During the experiments, the position of the contact line at a specific time was determined. Using image processing programs, composite images $pix\,1(t)$ were created for each step time t ($\Delta t = 30$ s) where the contact line position appeared at a gray level n_l on a black background (gray level 0). Then, for each time t, $pix\,0$ and $pix\,1(t)$ were added [16]. Figure 9 shows a part of a composite image created this way (the gray levels were modified for a better view). The parts of the contact line lying on defects appear with a gray level $n_d + n_l$ and the parts of the contact line lying on the matrix appear with a gray level $n_s + n_l$. Counting the number of pixels $N_r(t)$ on the resin and the number of pixels $N_s(t)$ on the silicon leads to the determination of the line fraction of defects $\chi(t)$ with

$$\chi = \frac{N_r}{N_r + N_s}. \tag{8}$$

The line fraction $\chi(t)$ along the contact line is a function of the position of the line $\mathcal{L}$ on the substrate. Experiments were performed varying the defect density on the substrate and measuring $\chi(t)$. Figure 10 shows the fluctuation of $\chi(t)$ on disordered substrates ($N_0 = 4$) with a defect size $d = 0.1$ mm for different densities of defects. The straight lines represent the mean line fraction χ_m associated with each substrate. The calculated χ_m (from Eq. (5)) fits correctly the experimental data except for a very low fraction of defects. For such coverage fractions, the distance between defects is several times the size of the defect. The triple line

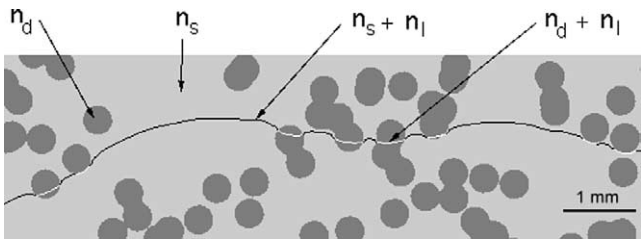

Fig. 9. Composite image of the contact line used to determine the line fraction of defect χ along the contact line $\mathcal{L}$.

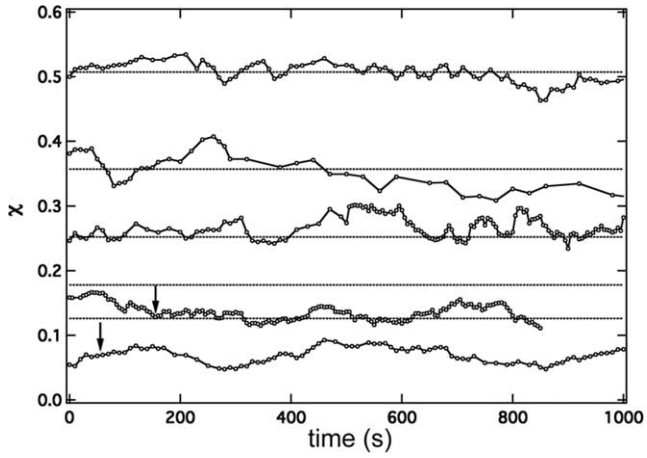

Fig. 10. Time evolution of the experimental line fraction χ ($d = 0.1$ mm). Solid lines are the mean line fraction χ_m associated with each substrate.

$\mathcal{L}_3$ cannot be digitally associated with a straight line and its radius of curvature R must be taken into account.

4.2. Apparent contact angle

The apparent contact angle on a heterogeneous surface is usually considered to be predictable by the Cassie equation [17]. This approach to the problem is based on the work of cohesion of the drop on the surface. For a surface composed of i types of solids, considering a mean field approach of the total work of cohesion W of the drop on the composite surface and using Eq. (1) on each solid i, W is

$$W = \sum_i \sigma_i (\gamma_{\mathrm{sg},i} + \gamma - \gamma_{\mathrm{sl},i}) = \gamma \sum_i \sigma_i (1 + \cos\theta_i), \tag{9}$$

where σ_i is the surface fraction of the solid i with respect to the entire surface ($\sum_i \sigma_i = 1$). The apparent contact angle associated with W is

$$\cos\theta_m = \sum_i \sigma_i \cos\theta_i, \tag{10}$$

where θ_i is the contact angle on the solid i. This phenomenological equation cannot be theoretically applied when the heterogeneities are at molecular size [18] or when the size of the drop is far below the capillary length because the line tension has to be taken into account [19].

Spreading experiments of large drops on ordered and disordered surfaces ($0 < N_0 < 4$) were performed. We investigated the influence of a surface density σ ranging from 0 to 1. At the end of each experiment, the thickness h_m of the drop was measured at different points near the center of the drop to determine the apparent contact angle θ_m using Eq. (2). The data are reported in Fig. 11. The relative dispersion in the values of the measured contact angles expresses the hysteresis of the process. The thickness depends on the position of the contact line. The solid line is the Cassie equation for two solids:

$$\cos\theta_m = \sigma \cos\theta_r + (1 - \sigma)\cos\theta_s. \tag{11}$$

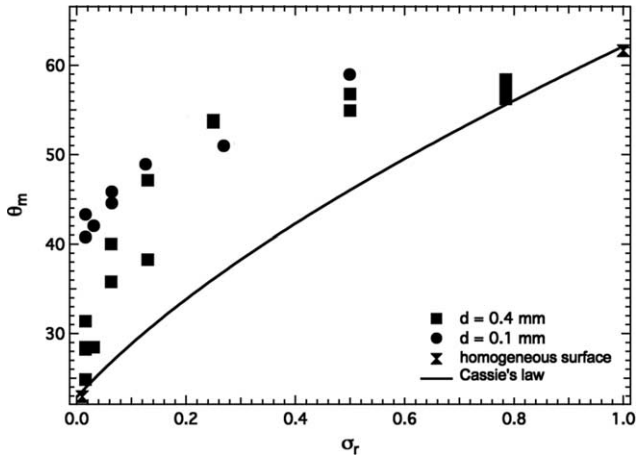

Fig. 11. Experimental apparent contact angle vs surface fraction of defects.

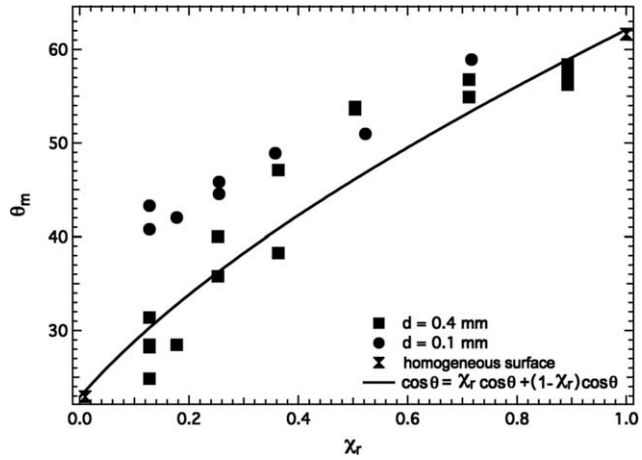

Fig. 12. Experimental apparent contact angle vs line fraction of defects.

As can be seen Fig. 11, Eq. (11) does not fit the experimental points. Numerous studies [20–24] relate experimental apparent contact angles to Eq. (11). Depending on the definition of the degree of heterogeneity σ results match more or less successfully Eq. (11). Modified Cassie equations were proposed, with additional terms taking into account the contour length per unit area between different materials [24] or additional terms taking into account the ratio of the fractional length of the contact line on each material and the line tension [19,25]. However, in the case of large defects ($d > 20$ μm), the effect of line tension is negligible [26]. The use of the surface fraction of defects σ in the prediction of the apparent contact angle on a heterogeneous surface is questionable as the value of the contact angle depends on the surface properties along the contact line $\mathcal{L}$. In our system, the size of the defects d is far larger than the contact line width δ; hence the use of the surface fraction of defects σ is inadequate to characterize the surface properties to quantify the apparent contact angle. However, the same mean field approach of the work of cohesion W of the drop on the composite surface can be made using the line fraction χ instead of the surface fraction σ. During the spreading, as the line fraction χ along the contact line fluctuates around the mean value χ_m, the apparent contact angle can be expressed using the contact angles on the two surfaces and χ_m:

$$\cos\theta_m = \chi_m \cos\theta_r + (1 - \chi_m)\cos\theta_s. \tag{12}$$

In Fig. 12, the experimental apparent contact angles are reported on the different surfaces characterized by their mean line fraction of defects χ_m. The solid line (Eq. (12)) fits the experimental data reasonably well. While this approach assumes that $\theta_4 = \theta_r$, i.e., the four-phase line is neglected ($g(t) = 1$), the comparison with the experiments is acceptable.

5. Summary

The local geometry of wettability defects is considered as a cause of contact angle modification in the case of large drops spreading on solid surfaces. Wettability defects deform the drop edge on a distance larger than their size. As a function of the distance between defects, individual pinning and collective pinning occur. The contact line radius of curvature between two defects is shown to increase linearly with the distance between the edge of the defects. Experiments in wettability channels with ordered and disordered distributions of defects show the possibility of defining a single value of the apparent advancing contact angle for a given defect density that does not depend on the nature of the disorder. The line fraction of defects along the contact line is studied during spreading experiments. Measured contact angles follow a Cassie-type law when plotted versus the density of defects. When the density of defects is defined in terms of fraction of the contact line on defects and on the matrix, the experimental data are well described by a modified Cassie equation.

Acknowledgments

We acknowledge financial support from Institut Français du Pétrole. The patterned substrates were prepared in Laboratoire de Microélectronique et Microstructures du CNRS with the help of D. Mailly. We also thank P. Jenffer for technical assistance and L. Limat and M. Barquins for fruitful discussions. We are grateful to one of the referees for suggesting Eq. (7).

References

[1] A.A. Darhuber, S.M. Troian, J. Appl. Phys. 90 (2001) 3602–3609.
[2] A. Martin, O. Rossier, A. Buguin, P. Auroy, F. Brochard-Wyart, Eur. Phys. J. E 3 (2000) 337–341.
[3] H. Gau, S. Herminghaus, P. Lenz, R. Lipowsky, Science 283 (1999) 46–49.
[4] T. Smith, G. Lindberg, J. Colloid Interface Sci. 66 (1978) 363–366.
[5] C. Andrieu, C. Sykes, F. Brochard, Langmuir 10 (1994) 2077–2080.
[6] J. Marsh, A. Cazabat, Phys. Rev. Lett. 71 (1993) 2433–2436.

[7] G. Nadkarni, S. Garoff, Europhys. Lett. 20 (1992) 523–528.
[8] J.-M. di Meglio, Europhys. Lett. 17 (1992) 607–612.
[9] A. Paterson, M. Fermigier, Phys. Fluids 9 (1997) 2210.
[10] D. Chatain, V. de Jonghe, J. Adhes. 58 (1996) 163–171.
[11] A. Prevost, E. Rolley, C. Guthmann, Phys. Rev. Lett. 83 (1999) 348–351.
[12] P.-G. de Gennes, Rev. Mod. Phys. 57 (1985) 827–863.
[13] T. Cubaud, M. Fermigier, Europhys. Lett. 55 (2001) 239–245.
[14] T. Cubaud, M. Fermigier, Oil Gas Sci. Technol. Rev. IFP 56 (2001) 23–31.
[15] A. Tanguy, M. Gounelle, S. Roux, Phys. Rev. E 58 (1998) 1577–1590.
[16] A. Jain, Fundamentals of Digital Image Processing, Prentice Hall, New York, 1989.
[17] A. Cassie, S. Baxter, S. Trans. Faraday Soc. 40 (1944) 546.
[18] J. Israelachvili, M. Gee, Langmuir 5 (1989) 288–289.
[19] J. Drelich, J.L. Wilbur, J.D. Miller, G.M. Whitesides, Langmuir 12 (1996) 1913–1922.
[20] D. Oner, J. McCarthy, Langmuir 16 (2000) 7777–7782.
[21] W.J. Herzberg, J.E. Marian, T. Vermeulen, J. Colloid Interface Sci. 33 (1970) 164–171.
[22] R. Dettre, R. Johnson, J. Physical Chemistry 69 (1965) 1507–1515.
[23] S. Semal, M. Voué, M.J. de Ruijter, J. Dehuit, J.D. Coninck, J. Phys. Chem. B 103 (1999) 4854–4861.
[24] J.T. Woodward, H. Gwin, D.K. Schwartz, Langmuir 16 (2000) 2957–2961.
[25] J. Drelich, Polish. J. Chem. 71 (1997) 525–549.
[26] J. Buehrle, S. Herminghaus, F. Mugele, Langmuir 18 (2002) 9771–9777.